Outstanding Enhancement in the Axial Coordination Ability of the Highly Rigid Cofacial Cyclic Metalloporphyrin Dimer

Ken-ichi Yamashita,* Kazuhiro Furutani and Takuji Ogawa

[a] Dr. K. Yamashita, K. Furutani, Prof. Dr. T. Ogawa
Department of Chemistry, Graduate School of Science
Osaka University
1-1 Machikaneyama, Toyonaka, Osaka 560-0043, Japan
E-mail: yamashita-k@chem.sci.osaka-u.ac.jp

Supporting information for this article is given via a link at the end of the document.

Abstract: Copper- and nickel-porphyrin complexes show extremely weak axial coordination ability without any electron-withdrawing groups. Herein, we report axial ligation on Cu^{II}- and Ni^{II}-porphyrins in a highly rigid cofacial porphyrin dimer with a bidentate ligand, 1,4-diazabicyclo[2.2.2]octane (DABCO). To the best of our knowledge, this is the first report on the use of Cu^{II}- and Ni^{II}-porphyrins for coordination-induced guest binding of porphyrin-based host molecules without the help of other metal ions. The high rigidity of the dimer induces guest binding through the cooperative effect of weak axial ligation. The results showed that Cu^{II}- and Zn^{II}-complexes bind one DABCO molecule inside their cavities, whereas the Ni^{II}-complex binds two additional DABCO molecules outside to form a stable 6-coordinate paramagnetic Ni^{II}-complexes. The binding constants were determined by the UV/vis titration experiments.

Introduction

The coordination of ligands to a porphyrin central metal is important for many biological reactions, catalysis, and supramolecular chemistry.[1] In porphyrin supramolecular chemistry, axial coordination is responsible for including a guest molecule into the cavity of (multi)porphyrin-based host molecules.[2,3] In addition, large and discrete multi-metalloporphyrin macrocycles or cages have been fabricated by template synthesis, which involves the preorganization of porphyrin monomers by axial coordination of well-designed multidentate ligands.[2,4–10]

The coordination ability and the maximum coordination number chiefly depend on the metal ion.[1,11,12] For example, zinc porphyrins exhibit a high axial coordination ability to oxygen- and nitrogen-based ligands and readily form a five-coordinate complex.[11] Similarly, magnesium and cobalt porphyrins also exhibit a high axial coordination ability. These metals are commonly used for designing porphyrin-based host molecules that can bind guest molecules through axial coordination. Compared to these metalloporphyrins, nickel and copper porphyrins exhibit a weaker coordination ability with small binding constants (K_1 = 1.08 M^{-1}, K_2 = 3.79 M^{-1} for Ni^{II}(tpp) (tpp = tetraphenylporphyrinato dianion) with two pyrrolidine ligands,[11,13] and K_1 = 0.05 M^{-1} for Cu^{II}(tpp) with one pyridine ligand).[11,14–17] Therefore, typical Cu^{II}- and Ni^{II}-porphyrins do not exhibit axial coordination in the presence of slight excess of an axial ligand.

A conventional strategy for enhancing the axial coordination ability of these metal ions is to increase their Lewis acidity by introducing electron-withdrawing substituents on the periphery of the porphyrin.[13,18–26] For example, the nickel tetrakis(pentafluorophenyl)porphyrin complex readily accepts two axial ligands to form paramagnetic 6-coordinate complexes (K_1 = 8.2 M^{-1}, K_2 = 22.4 M^{-1}).[22] Analogous highly electron-deficient tetrapyrrole ligands have been also reported.[27–32]

The cooperative effect of multiple metal ions is also expected to efficiently induce axial coordination. In general, the cooperative binding of a suitable combination of a porphyrin host and a guest ligand is entropically more favorable than that of the corresponding monomer. In particular, structurally rigid multiporphyrin hosts in which the porphyrin units are strongly fixed exhibit significantly higher binding constants for guest molecules of the appropriate size.[2–4,7–9] However, to date, the cooperative effect has not been used to induce axial coordination in metalloporphyrins with a weak binding ability (e.g., Ni^{II} and Cu^{II}), except for one recent report by Anderson et al.[17,33] They reported axial ligation on copper porphyrins without any electron-withdrawing substituents in the heterometallic (Cu^{II}/Zn^{II}) cyclic porphyrin oligomers with a radial oligopyridyl ligand. This unusual ligation on Cu^{II} porphyrin units induced a cooperative strong ligation on Zn porphyrin units. To the best of our knowledge, there are no reports on guest inclusion by only axial ligation on Ni^{II} or Cu^{II} porphyrin units.

In this study, we investigate axial ligation on Ni^{II} and Cu^{II} porphyrins in a highly rigid cofacial porphyrin dimer[3] with a bidentate ligand without using electron-withdrawing substituents or strongly coordinating metal ions such as Zn^{II} porphyrins. (Figure 1). We have earlier reported the efficient synthesis of a cofacial porphyrin dimer bridged by two 2,7-naththyleneoxy-linkers (**1**)[34] via catalyst-free nucleophilic aromatic substitution reactions.[35–38][39–47] This dimer has a highly rigid structure, as revealed by the diffraction and spectroscopic studies, and has an internal cavity surrounded by two porphyrin moieties with an interplanar distance of ~7.5 Å, which is suitable for binding a 1,4-diazabicyclo[2.2.2]octane (DABCO) molecule. Therefore, we anticipated that the high rigidity of **1** can realize axial coordination of DABCO on the metal complexes (M = Zn^{II}, Cu^{II}, and Ni^{II}) of **1**. In fact, we were able to achieve the inclusion of DABCO in Cu^{II}-**1** and Ni^{II}-**1**.

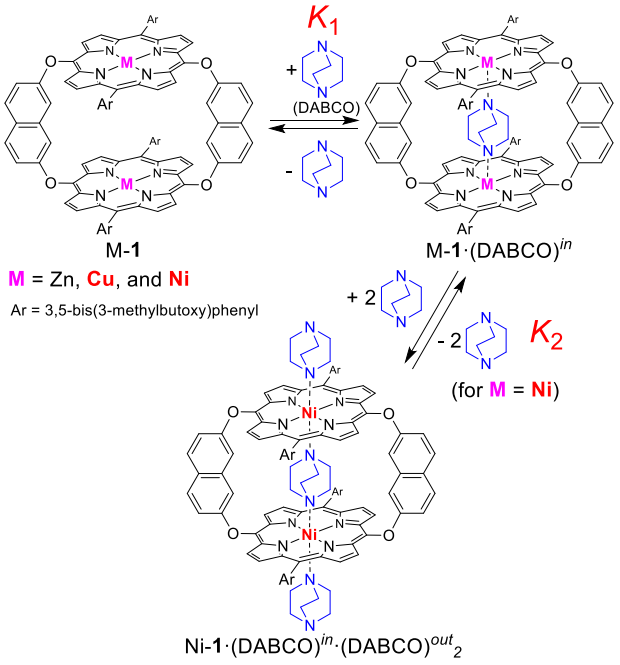

Scheme 1. Axial-coordination-driven inclusion of DABCO into M-**1**.

Results and Discussion

First, we evaluated the guest binding behavior of Zn^{II}-**1** with DABCO. As expected, when DABCO is added in a solution of Zn^{II}-**1,** the DABCO molecules were quickly bound in Zn^{II}-**1** to form Zn^{II}-**1**·(DABCO)^{in}. Zn^{II}-**1**·(DABCO)^{in} exhibited extraordinary stability even on silica gel. Thin-layer chromatography (TLC, hexane/toluene 1:3) analyses showed that Zn^{II}-**1**·(DABCO)^{in} (R_f = 0.9) has a different spot from that of unbound Zn^{II}-**1** (R_f = 0.4). Moreover, 2D TLC analyses indicated that the amount of unbound Zn^{II}-**1** was mostly negligible (Figure S9). Therefore, Zn^{II}-**1**·(DABCO)^{in} can be purified by both the typical column chromatography and recrystallization techniques.[9,48]

The ^{1}H NMR spectra of purified Zn^{II}-**1**·(DABCO)^{in} in $CDCl_3$ showed a sharp singlet proton signal for the bound DABCO molecule at −4.3 ppm, which are significantly upfield-shifted compared to that of free DABCO because of the magnetic shielding by two aromatic porphyrin macrocycles. When both Zn^{II}-**1** and Zn^{II}-**1**·(DABCO)^{in} exist in the solution, their ^{1}H NMR signals were independently observed without any shifts and broadening (Figure S10). Moreover, any change in the ^{1}H NMR spectra of Zn^{II}-**1**·(DABCO)^{in} was mostly negligible even in the presence of guest molecules, and both bound and excess free DABCO peaks were independently observed (Figure S10). These results indicate that the binding and release of DABCO has a slower timescale at room temperature than the NMR timescale. The results also show the high thermodynamic and kinetic stability of Zn^{II}-**1**·(DABCO)^{in}. Notably, the overall D_{2h} symmetry of Zn^{II}-**1** is retained even after the binding of DABCO with D_{3h} symmetry. This phenomenon indicates fast rotation of the DABCO molecule along the Zn^{II}–N···N–Zn^{II} axis inside the cavity of Zn^{II}-**1**, which is typical of the reported DABCO-coordinated Zn^{II}-porphyrin hosts.[48–54]

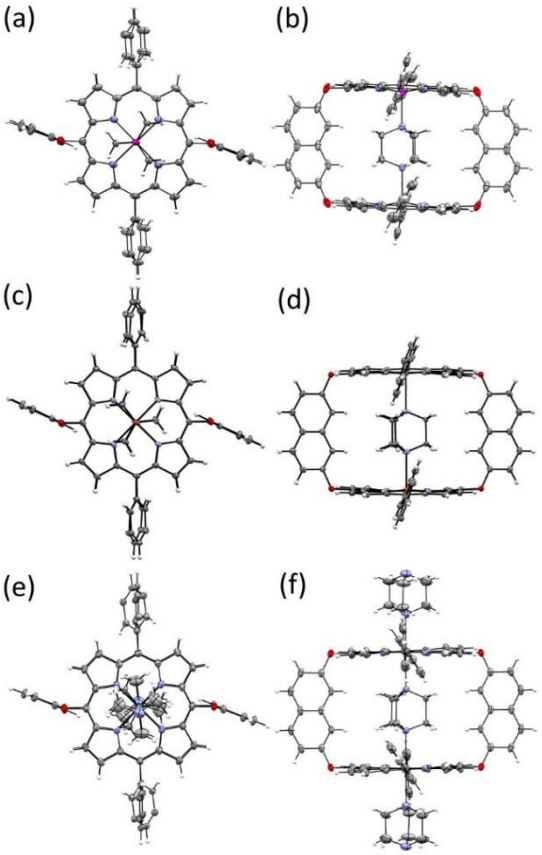

Figure 1. Thermal ellipsoid representations (40% probability level) of the crystal structure of M-**1**·(DABCO)^{in}. (a) Top and (b) side views of Zn^{II}-**1**·(DABCO)^{in}, (c) top and (d) side views of Cu^{II}-**1**·(DABCO)^{in}, and (e) top and (f) side views for the crystal structure of Ni^{II}-**1**·(DABCO)^{in}·(DABCO)$^{out}{}_2$. C = gray, H = white, N = blue, O = red, Zn = purple, Cu = brown, and Ni = green. Substituents on the phenyl groups and solvated molecules are omitted for clarity. The bound DABCO molecules were disordered at the two sites with half occupancy, and one site is shown. For Zn^{II}-**1**, two crystallographically independent but structurally similar molecules existed in the crystal, and therefore, only one molecule is shown.

Table 1. Selected structural data.

	Zn[e]	Cu	Ni
M–N_{DABCO}	2.197(2), 2.207(2)	2.428(2)	2.411(3), 2.407(3) [f]
$(M–N_{pyrrole})_{av}$ / Å	2.062, 2.064	2.013	2.033
M–P_{porN4} / Å[a]	0.289, 0.300	0.123	0.007
M···M / Å [b]	6.9723(7), 7.0090(5)	7.451(1)	7.4486(8)
P_{por24}···P_{por24} / Å[c]	7.553, 7.608	7.680	7.455
mpd / Å [d]	0.0537, 0.0653	0.0611	0.0803

[a] The vertical distance between metal ion and the mean plane defined by four N atoms of the porphyrin macrocycles. [b] The intramolecular M···M distance. [c] The interplane distance between two porphyrin macrocycles. The mean plane was defined by the core 24 atoms of the porphyrin macrocycles. [d] Mean plane deviation defined by the core 24 atoms. [e] Two crystallographically independent molecules existed in the crystal, and therefore, both values are shown. [f] M–$N_{DABCO\text{-}in}$ and M–$N_{DABCO\text{-}out}$, respectively.

The structure of Zn^{II}-**1**·(DABCO)$_{in}$ was confirmed by X-ray crystallography (Figures 1a,b and S2, Tables 1 and S1). As expected, one DABCO molecule was bound in the cavity of Zn^{II}-**1** by axial coordination on both nitrogen atoms of the guest molecules to the zinc ions. The overall structure was relatively similar to that of **1** reported previously.[34] The Zn^{II}–N_{DABCO} bond length was ~2.20 Å, slightly longer than the Zn^{II}–N_{por} bond length (~2.06 Å). The Zn ions were located 0.29–0.30 Å off the mean plane comprising four nitrogen atoms. Therefore, the Zn^{II} ions had distorted square-pyramidal geometry. These structural features are identical to those of the reported DABCO-coordinated Zn^{II}-porphyrin hosts.[48–51]

To estimate the binding constants between Zn^{II}-**1** and DABCO, UV/vis titration experiments were carried out (Figure 2). When DABCO is added to the solution of Zn^{II}-**1** in chlorobenzene, both Soret and Q bands red-shifted, indicating axial coordination of DABCO on the Zn ions of porphyrins. The end-point of the spectral change is reached when one equivalent of DABCO molecules is added to the solution of Zn^{II}-**1** in chlorobenzene. However, the value of the obtained K_1 value shows a large deviation from that determined by nonlinear curve fitting (K_1 = 7.2±17.5)×10^9 M^{-1}), probably because it is difficult to directly determine a high binding constant (>10^8) by UV/Vis titration.[7,55]

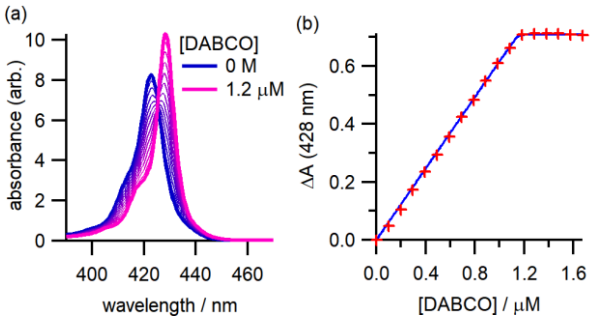

Figure 2. (a) UV/vis spectral change of the Soret band of Zn^{II}-**1** (1.15 μM) upon adding DABCO (0–1.2 μM) in chlorobenzene at 298 K. (b) Titration curve of Zn^{II}-**1** with DABCO monitored at 429 nm. The solid line represents the best fitting curve.

We then evaluated the guest binding behavior of Cu^{II}-**1**. The UV/vis titration experiment showed that Cu^{II}-**1** also bind DABCO to form Cu^{II}-**1**·(DABCO)$_{in}$ (Figure 3). Upon adding DABCO, both Soret and Q bands of Cu^{II}-**1** red-shifted. Similar to that of Zn^{II}-**1**, Cu^{II}-**1** shows isosbestic points, suggesting the formation of a 1:1 host–guest complex, Cu^{II}-**1**·(DABCO)$_{in}$. Binding constant K_1 was determined to be 928±10 M^{-1} by nonlinear curve fitting.

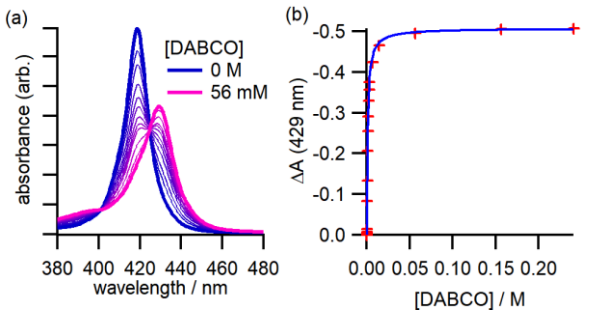

Figure 3. (a) UV/vis spectral change of the Soret band of Cu^{II}-**1** (1.08 μM) upon the addition of DABCO in chlorobenzene at 298 K. (b) Titration curve of Cu^{II}-**1** with DABCO monitored at 429 nm. The solid line represents the best fitting curve.

The structure of Cu^{II}-**1**·(DABCO)$_{in}$ was elucidated by X-ray crystallography (Figure 1c,d). The cavity of Cu^{II}-**1** had one DABCO molecule. The two porphyrin macrocycles retained their planarity with a small mean plane deviation 0.06 Å for the 24 core atoms. The Cu–N_{DABCO} bond length was 2.428(2) Å, which was considerably longer than the Cu–N_{por} bond length (2.013 Å). Such a long bond length is characteristic of the d9 metal ion. The Cu^{II} ions were located 0.12 Å off the mean plane core comprising four nitrogen atoms, a shorter distance than that between Zn^{II}-**1** and the nitrogen atoms. Therefore, the interplane distance between two porphyrin macrocycles was relatively similar between Zn^{II}-**1** and Cu^{II}-**1** despite the different M–N_{DABCO} bond lengths.

To evaluate the structural effect of highly rigid Cu^{II}-**1**, a titration experiment was also performed on the flexible acyclic dimer Cu^{II}-**2**[34] and monomer Cu^{II}-**3** (Figure 4). A slight spectral change was observed with Cu^{II}-**2**, even when the DABCO concentration was 0.5 M. No spectral change was observed when the DABCO concentration was 1.3 M. This result is acceptable considering the extremely small binding constants of Cu^{II} porphyrins.[14–17] Hence, it can be concluded that the significant rigidity of **1** induces guest binding through cooperative effect of the weak axial ligation on Cu^{II} ions.

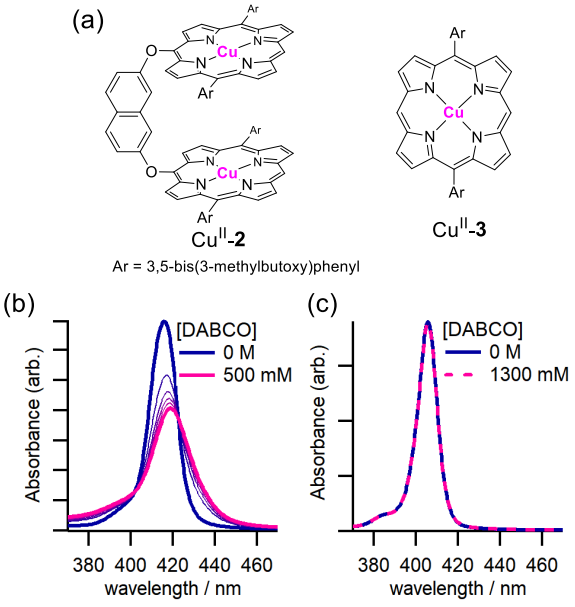

Figure 4. (a) Chemical structures of the reference compounds. UV/vis spectral change of the Soret band of (b) Cu^{II}-**2** and (c) Cu^{II}-**3** upon the addition of DABCO in chlorobenzene at 298 K.

To explore the scope of this approach to induce unusual axial ligation, the binding of DABCO in the Ni^{II}-**1** complexes was evaluated. As expected, Ni^{II}-**1** exhibited the binding of DABCO molecules revealed by UV/vis titration experiments. Contrary to the spectral change in Zn^{II}-**1** and Cu^{II}-**1**, that in Ni^{II}-**1** does not have any isosbestic points (Figure 5a). This result suggests that

more than three species are involved in the titration. Considering that Ni^{II}-porphyrins generally favor two-ligand coordination to form octahedral 6-coordinate Ni^{II} species instead of one-ligand coordination,[13,18–23] two additional DABCO molecules bind outside and one inside the cavity of Ni^{II}-**1** to form Ni^{II}-**1**·$(DABCO)^{in}$·$(DABCO)^{out}_2$ (Scheme 1).

The structure of the Ni^{II}-**1**·$(DABCO)^{in}$·$(DABCO)^{out}_2$ complex comprising three DABCO molecules was unambiguously determined by X-ray diffraction (Figure 1e and f). The $Ni–N_{DABCO\text{-}in}$ and $Ni–N_{DABCO\text{-}out}$ bond lengths were 2.411(3) and 2.407(3) Å, respectively. These bond lengths were considerably longer than those of $Ni–N_{por}$ (2.033 Å), and slightly longer than those of 6-coordinate octahedral Ni-porphyrinoid complexes (2.2–2.3 Å).[19,20,22,27,28,32,56] The Ni ions were located mostly on the mean plane core comprising four nitrogen atoms.

The binding constants were determined from the UV/vis titration experiment (Figure 5b). To simplify the fitting model, we postulated a single-step formation of Ni^{II}-**1**·$(DABCO)^{in}$·$(DABCO)^{out}_2$ from Ni^{II}-**1**·$(DABCO)^{in}$ with one equilibrium constant (K_2). K_1 and K_2 were determined to be 2.84±0.22 M^{-1} and 132±15 M^{-2}, respectively.

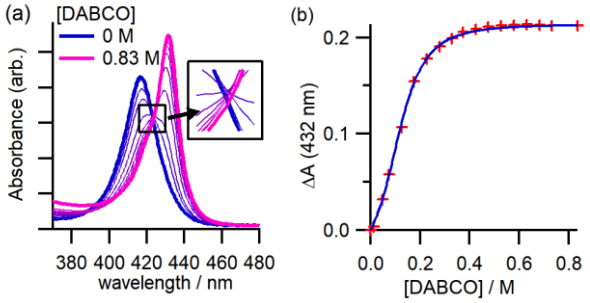

Figure 5. UV/vis spectral change of the Soret band of Ni^{II}-**1** (1.01 μM) upon the addition of DABCO (0–0.83 M) in chlorobenzene at 298 K.

Axial coordination on the Ni^{II} ion in the porphyrins induces spin change from diamagnetic to paramagnetic.[18,22,23,28,32,56–59] This phenomenon was also observed in the DABCO binding in Ni^{II}-**1**. While the ^{1}H NMR signals of β-protons for free Ni^{II}-**1** was observed within the range of typical diamagnetic compounds (8.89 and 8.53 ppm in $CDCl_3$), those of Ni^{II}-**1** in the presence of DABCO appeared significantly downfield (51.9 and 49.6 ppm) (Figure S11). This behavior is the characteristic of the reported 6-coordinated Ni^{II}-porphyrins and clearly indicates the paramagnetic character of Ni^{II}-**1**·$(DABCO)^{in}$·$(DABCO)^{out}_2$.

Conclusion

We demonstrated the unusual axial coordination on Cu^{II} and Ni^{II} ions on the cofacial cyclic porphyrin dimer. Its remarkably high rigidity enhanced its cooperative axial ligation ability. To the best of our knowledge, this is the first report on the use of Cu^{II}- and Ni^{II}-porphyrins for coordination-induced guest binding of porphyrin-based host molecules without using other metal ions. Different metal complexes with various anomalous coordination forms, such as relatively rare 5- or 6-coordinated Pd^{II} species that are difficult to prepare in solution, can be synthesized by utilizing the strategy presented herein. The syntheses of such complexes with an abnormal coordination mode and investigation of their properties are underway and the results will be reported in due time.

Experimental Section

Instrumentation and Materials

Bis(2,7-naphthylenedioxy)-bridged cyclic porphyrin dimer (**1**),[34] mono-bridged acyclic porphyrin dimer (**2**),[34] and reference monomer (**3**)[60] were synthesized as previously reported procedures. Chlorobenzene (PhCl) was distilled from CaH_2. All other chemicals were of reagent grades and used without any further purification. $CDCl_3$ was acquired from Cambridge Isotope Laboratories, Inc. Analytical thin layer chromatography (TLC) was performed on silica gel 60 F_{254} plates. Flash column chromatography was performed using silica gel 60N (spherical, neutral, 40–50 μm). NMR spectral data were recorded on a JEOL ECS500 spectrometers. These data were collected at ambient temperature (25 °C). ^{1}H NMR spectra were referenced internally to tetramethylsilane as a standard. ^{13}C NMR spectra were referenced internally to a solvent signal (δ = 77.0 ppm for $CDCl_3$). IR measurements were recorded on a JASCO FT/IR-6100 spectrometer equipped with an ATR unit. UV/Vis spectral data were recorded on a SHIMADZU UV-3150 spectrometer.

Synthesis of Zn^{II}-1

A mixture of **1** (100.1 mg, 0.0520 mmol) and $Zn(OAc)_2·2H_2O$ (114.5 mg, 0.522 mmol) in $CHCl_3$ (6 mL) and MeOH (0.6 mL) was stirred at room temperature for 2 h. The reaction mixture was directly poured on top of a basic alumina column packed with $CHCl_3$, then eluted with $CHCl_3$. The solvent was removed under reduced pressure to give Zn^{II}-**1** as purple powder (100.4 mg, 0.0489 mmol, 94%). Analytically pure product was obtained by the recrystallization from hot toluene–hexane. R_f = 0.37 (silica gel, hexane/toluene = 1:3); m.p. >300 ºC; ^{1}H NMR (500 MHz, $CDCl_3$) δ = 9.00 (d, J = 4.6 Hz, 8H), 8.68 (d, J = 4.2 Hz, 8H), 8.03 (d, J = 8.8 Hz, 4H), 7.92 (dd, J = 9.4, 2.5 Hz, 4H), 7.11 (t, J = 1.5 Hz, 4H), 6.85 (t, J = 1.5 Hz, 4H), 6.74 (t, J = 2.3 Hz, 4H), 4.41 (d, J = 2.7 Hz, 4H), 4.01–3.96 (m, 16H), 1.87–1.72 (m, 16H), 1.64 (q, J = 6.8 Hz, 8H), 1.01 (d, J = 6.9 Hz, 24H), 0.88 ppm (d, J = 6.5 Hz, 24H); ^{13}C NMR (125 MHz, $CDCl_3$) δ = 164.9 (*C*q), 158.4 (*C*q), 157.7 (*C*q), 149.2 (*C*q), 145.7 (*C*q), 143.1 (*C*q), 134.8 (*C*q), 132.5 (*C*H), 131.4 (*C*q), 129.3 (*C*H), 127.3 (*C*H), 124.6 (*C*q), 120.8 (*C*q), 116.2 (*C*H), 115.0 (*C*H), 113.8 (*C*H), 111.2 (*C*H), 101.0 (*C*H), 66.8 (CH_2), 66.6 (CH_2), 38.1 (CH_2), 37.8 (CH_2), 25.2 (*C*H), 24.9 (*C*H), 22.9 (CH_3), 22.5 ppm (CH_3); IR (ATR): $\tilde{\nu}$ = 2952, 2867, 2365, 1629, 1586, 1511, 1430, 1384, 1350, 1328, 1183, 1155, 1031, 1002, 941, 866, 831, 794, 718 cm^{-1}; UV/Vis (chlorobenzene): λ_{max} (Logε) = 423 (5.91), 517 (3.76), 553.5 (4.53), 596 nm (3.99); elemental analysis calcd (%) for $C_{124}H_{128}N_8O_{12}Zn_2$: C, 72.54; H, 6.28; N, 5.46; found: C, 72.23; H, 6.20; N, 5.38.

Synthesis of Cu^{II}-1

A mixture of **1** (31.6 mg, 0.0164 mmol) and $Cu(OAc)_2·H_2O$ (33.6 mg, 0.168 mmol) in $CHCl_3$ (2 mL) and MeOH (0.2 mL) was stirred at room temperature for 0.5 h. The reaction mixture was directly poured on top of a silica gel column packed with $CHCl_3$, then eluted with $CHCl_3$. The solvent was removed under reduced pressure to give Cu^{II}-**1** as reddish purple powder (32.6 mg, 0.0159 mmol, 97%). Analytically pure product was obtained by the recrystallization from hot toluene–hexane. R_f = 0.20 (silica gel, hexane/$CHCl_3$ = 3:2); m.p. >300 ºC; IR (ATR): $\tilde{\nu}$ = 2952, 2868, 2364, 1630, 1587, 1512, 1451, 1432, 1383, 1354, 1336, 1245, 1222, 1187, 1161, 1064, 1006, 866, 831, 795, 716 cm^{-1}; UV/Vis (chlorobenzene): λ_{max} (Logε) = 417 (5.63), 531 nm (4.50); elemental analysis calcd (%) for $C_{124}H_{128}N_8O_{12}Cu_2$: C, 72.67; H, 6.30; N, 5.47; found: C, 72.42; H, 6.20; N, 5.46.

Synthesis of Ni^{II}-1

A mixture of **1** (53.0 mg, 0.0275 mmol) and $Ni(acac)_2$ (1133.3 mg, 0.556 mmol) in toluene (6 mL) was refluxed for 16 h. The reaction mixture was directly poured on top of a silica gel column packed with $CHCl_3$, then eluted with $CHCl_3$. The solvent was removed under reduced pressure to give Ni^{II}-1 as reddish purple powder (54.3 mg, 0.0266 mmol, 97%). Analytically pure product was obtained by the recrystallization from hot toluene–hexane. R_f = 0.74 (silica gel, hexane/CH_2Cl_2 = 1:2); m.p. >300 ºC; ^{1}H NMR (400 MHz, $CDCl_3$) δ = 8.89 (d, J = 4.9 Hz, 8H), 8.53 (d, J = 4.9 Hz, 8H), 8.01 (d, J = 9.0 Hz, 4H), 7.86 (dd, J = 9.2, 2.4 Hz, 4H), 7.20 (brs, 4H), 6.69 (t, J = 2.2 Hz, 4H), 6.52 (brs, 4H), 4.88 (d, J = 2.4 Hz, 4H), 4.01 (t, J = 6.5 Hz, 8H), 3.89 (t, J = 6.6 Hz, 8H), 1.89–1.79 (m, 4H), 1.76–1.70 (m, 12H), 1.59 (q, J = 6.5 Hz, 8H), 0.99 (d, J = 6.4 Hz, 24H), 0.85 ppm (d, J = 6.4 Hz, 24H); ^{13}C NMR (125 MHz, $CDCl_3$) δ = 163.0 (*C*q), 158.6 (*C*q), 158.1 (*C*q), 142.5 (*C*q), 142.0 (*C*q), 139.3 (*C*q), 134.8 (*C*q), 132.4 (*C*H), 130.7 (*C*q), 129.6 (*C*H), 127.2 (*C*H), 124.9 (*C*q), 119.3 (*C*q), 116.4 (*C*H), 113.3 (*C*H), 110.6 (*C*H), 101.0 (*C*H), 66.7 (CH_2), 66.5 (CH_2), 38.1 (CH_2), 37.9 (CH_2), 25.2 (*C*H), 24.9 (*C*H), 22.7 (CH_3), 22.5 ppm (CH_3); IR (ATR): $\tilde{\nu}$ = 2926, 2869, 2363, 1631, 1587, 1464, 1450, 1346, 1313, 1247, 1124, 1120, 1165, 1135, 1065, 1010, 971, 956, 866, 830, 822, 795, 771, 722, 694 cm^{-1}; UV/Vis (chlorobenzene): λ_{max} (Logε) = 417 (5.63), 531 nm (4.50); MS(MALDI-TOF): *m/z* 1762.98 ([*M*+H]$^+$); elemental analysis calcd (%) for $C_{124}H_{128}N_8O_{12}Ni_2$: C, 73.01; H, 6.33; N, 5.49; found: C, 72.85; H, 6.20; N, 5.52.

Synthesis of Cu^{II}-2

Cu^{II}-**2** was synthesized in a similar manner to that of **Cu^{II}-1**. Analytically pure product was obtained by the recrystallization from hot ethyl acetate. UV/Vis (chlorobenzene): λ_{max} = 416, 536 nm; elemental analysis calcd (%) for $C_{114}H_{124}N_8O_{10}Cu_2$·(EtOAc): C, 71.53; H, 6.71; N, 5.66; found: C, 71.41; H, 6.59; N, 5.96.

Synthesis of Cu^{II}-3

Cu^{II}-**3** was synthesized in a similar manner to that of **Cu^{II}-1**. Analytically pure product was obtained by the recrystallization from CH_2Cl_2–methanol. UV/Vis (chlorobenzene): λ_{max} = 405.5, 528, 562 nm; elemental analysis calcd (%) for $C_{52}H_{60}N_4O_4Cu$: C, 71.90; H, 6.96; N, 6.45; found: C, 71.77; H, 6.99; N, 6.42.

X-Ray crystal structure determinations

Single crystals of [Zn^{II}-**1**·$(DABCO)^{in}$]·$(o\text{-}C_6H_4Cl_2)_2$ were obtained by the slow diffusion of methanol vapor into their solution in o-dichlorobenzene. Single crystals of [Cu^{II}-**1**·$(DABCO)^{in}$]·$(DABCO)$·$(CH_3CN)_2$ were obtained by layering of a o-dichlorobenzene solution of Cu^{II}-**1** and DABCO (excess) with a saturated acetonitrile solution of DABCO. Single crystals of [Ni^{II}-**1**·$(DABCO)^{in}$·$(DABCO)^{out}{}_2$]·$(C_6H_5Cl)_2$·$(H_2O)_2$ were obtained by the slow diffusion of methanol vapor into a chlorobenzene solution of Ni^{II}-**1** and DABCO (excess).

Single-crystal X-ray diffraction data were collected on a Rigaku XtaLAB Synergy Custom diffractometer using multilayer mirror monochromated Mo-Kα radiation (λ = 0.71075 Å) by the ω scan mode. The crystal was cooled by a stream of cold N_2 gas. Collection, indexing, peak integration, cell refinement, and scaling of the diffraction data were performed using CrysAlisPro 1.171.40.75a software (Rigaku OD, 2020). The data were corrected for Lorentz and polarization effects, and empirical absorption correction was applied. The structures were solved using SHELXT[61] programs and refined by full-matrix least-squares calculations on F^2 (SHELXL).[62] All non-hydrogen atoms were modeled anisotropically. All hydrogen atoms were placed in idealized positions and refined using a riding model [U_{iso}(H) = 1.2U_{eq}(C)].

The crystallographic data are summarized in Table S1. CCDC 2045500 (Zn), 2045501 (Cu), and 2045502 (Ni) contain the supplementary crystallographic data for this paper. The data can be obtained free of charge via www.ccdc.cam.ac.uk/data_request/cif.

Determination of binding constants

3 mL of the M-**1** solution was placed in a 1-cm quartz cell, and 3 μL of a chlorobenzene solution of DABCO was added to it using a micro-syringe. The resulting solution was stirred for 3 min at room temperature. Its UV/vis spectra were recorded at room temperature after each addition. The changes in absorption (ΔA) at 428 nm (for Zn^{II}), 429 nm (for Cu^{II}), and 432 nm (for Ni^{II}) as a function of the concentration of the guest molecules were plotted. The binding constants (see Scheme 1) were determined by a nonlinear curve fitting based on the following equation.

$$\Delta A = \frac{(A_\infty - A_0)([G]+[H]+K^{-1}-\sqrt{([G]+[H]+K^{-1})^2-4[H][G]})}{2[H]}$$ (for Zn^{II} and Cu^{II})

$$\Delta A = \frac{(A_\infty - A_0)(K_1[G]_0+K_1K_2[G]_0{}^3)}{1+K_1[G]_0+K_1K_2[G]_0{}^3}$$ (for Ni^{II})

where ΔA is the differential absorbance ($A - A_0$), A_0 is the absorbance of the initial solution, A_∞ is the absorbance of the final solution, $[G]_0$ (= $[G]_{free}$+$[G]_{bound}$) is the total concentration of the guest molecule (DABCO) in the solution, and $[H]_0$ (= $[H]_{free}$+$[H]_{bound}$) is the total concentration of the host molecule in the solution. In the equation for Ni^{II}, the same molar extinction coefficient between 5-coordinate and 6-coordinate complexes was assumed as these complexes were similar to other Ni^{II}-porphyrin analogs.[21,22,32] We also assumed that the synthesis of Ni^{II}-**1**·$(DABCO)^{in}$·$(DABCO)^{out}{}_2$ from Ni^{II}-**1**·$(DABCO)^{in}$ involved only one step with one equilibrium constant (K_2).

Acknowledgements

This work was supported by JSPS KAKENHI Grant Numbers JP17K14447 and JP25110002. The NMR, and X-ray diffraction measurements were performed at the Analytical Instrument Facility, Graduate School of Science, Osaka University.

Keywords: Cooperative effects • Coordination modes • Host-guest systems • Molecular recognition • Porphyrinoids

[1] J. K. Sanders, N. Bampos, Z. Clyde-Watson, S. L. Darling, J. C. Hawley, H. J. Kim, C. C. Mak, S. J. Webb, in *Porphyr. Handbook, Vol. 3* (Eds.: K.M. Kadish, K.M. Smith, R. Guilard), Academic Press, San Diego, **2000**, pp. 1–48.

[2] S. Durot, J. Taesch, V. Heitz, *Chem. Rev.* **2014**, *114*, 8542–8578.

[3] V. Valderrey, G. Aragay, P. Ballester, *Coord. Chem. Rev.* **2014**, *258–259*, 137–156.

[4] Y. Nakamura, N. Aratani, A. Osuka, *Chem. Soc. Rev.* **2007**, *36*, 831–845.

[5] T. Y. Cen, S. P. Wang, Z. Zhang, J. Wu, S. Li, *J. Porphyrins Phthalocyanines* **2018**, *22*, 726–738.

[6] S.-P. Wang, Y.-F. Shen, B.-Y. Zhu, J. Wu, S. Li, *Chem. Commun.* **2016**, *52*, 10205–10216.

[7] M. Hoffmann, C. J. Wilson, B. Odell, H. L. Anderson, *Angew. Chem. Int. Ed.* **2007**, *46*, 3122–3125.

[8] M. Hoffmann, J. Kärnbratt, M.-H. Chang, L. M. Herz, B. Albinsson, H. L. Anderson, *Angew. Chem. Int. Ed.* **2008**, *47*, 4993–4996.

[9] J. K. Sprafke, D. V Kondratuk, M. Wykes, A. L. Thompson, M. Hoffmann, R. Drevinskas, W.-H. Chen, C. K. Yong, J. Kärnbratt, J. E. Bullock, M. Malfois, M. R. Wasielewski, B. Albinsson, L. M. Herz, D. Zigmantas, D. Beljonne, H. L. Anderson, *J. Am. Chem. Soc.* **2011**, *133*, 17262–17273.

[10] M. C. O'Sullivan, J. K. Sprafke, D. V. Kondratuk, C. Rinfray, T. D. W. Claridge, A. Saywell, M. O. Blunt, J. N. O'Shea, P. H. Beton, M. Malfois, H. L. Anderson, *Nature* **2011**, *469*, 72–75.

[11] M. Tabata, J. Nishimoto, in *Porphyr. Handbook, Vol. 9* (Eds.: K.M. Kadish, K.M. Smith, R. Guilard), Academic Press, San Diego, **2000**, pp. 221–419.

[12] P. Hambright, *Chem. Commun.* **1967**, 470–471.

[13] F. A. Walker, E. Hui, J. M. Walker, *J. Am. Chem. Soc.* **1975**, *97*, 2390–2397.
[14] J. R. Miller, G. D. Dorough, *J. Am. Chem. Soc.* **1952**, *74*, 3977–3981.
[15] G. Szintay, A. Horváth, G. Grampp, *J. Photochem. Photobiol. A Chem.* **1999**, *126*, 83–89.
[16] G. Szintay, A. Horváth, *Inorganica Chim. Acta* **2001**, *324*, 278–285.
[17] J. Cremers, S. Richert, D. V. Kondratuk, T. D. W. Claridge, C. R. Timmel, H. L. Anderson, *Chem. Sci.* **2016**, *7*, 6961–6968.
[18] T. La, R. A. Richards, R. S. Lu, R. Bau, G. M. Miskelly, *Inorg. Chem.* **1995**, *34*, 5632–5640.
[19] S.-L. Jia, W. Jentzen, M. Shang, X.-Z. Song, J.-G. Ma, W. R. Scheidt, J. A. Shelnutt, *Inorg. Chem.* **1998**, *37*, 4402–4412.
[20] H. Duval, V. Bulach, J. Fischer, R. Weiss, *Inorg. Chem.* **1999**, *38*, 5495–5501.
[21] Y. Song, R. E. Haddad, S. L. Jia, S. Hok, M. M. Olmstead, D. J. Nurco, N. E. Schore, J. Zhang, J. G. Ma, K. M. Smith, S. Gazeau, J. Pécaut, J. C. Marchon, C. J. Medforth, J. A. Shelnutt, *J. Am. Chem. Soc.* **2005**, *127*, 1179–1192.
[22] S. Thies, C. Bornholdt, F. Köhler, F. D. Sönnichsen, C. Näther, F. Tuczek, R. Herges, S. I. Materials, A. Fluor-, S.- Aldrich, D. Core, *Chem. - Eur. J.* **2010**, *16*, 10074–10083.
[23] M. Dommaschk, F. Gutzeit, S. Boretius, R. Haag, R. Herges, *Chem. Commun.* **2014**, *50*, 12476–12478.
[24] T. Kaufmann, B. Shamsai, R. S. Lu, R. Bau, G. M. Miskelly, *Inorg. Chem.* **1995**, *34*, 5073–5079.
[25] A. A. Sinelshchikova, S. E. Nefedov, Y. Y. Enakieva, Y. G. Gorbunova, A. Y. Tsivadze, K. M. Kadish, P. Chen, A. Bessmertnykh-Lemeune, C. Stern, R. Guilard, *Inorg. Chem.* **2013**, *52*, 999–1008.
[26] M. Amati, E. J. Baerends, G. Ricciardi, A. Rosa, *Inorg. Chem.* **2020**, *59*, 11528–11541.
[27] M. Dommaschk, V. Thoms, C. Schütt, C. Näther, R. Puttreddy, K. Rissanen, R. Herges, *Inorg. Chem.* **2015**, *54*, 9390–9392.
[28] A. Yagi, T. Kondo, D. Yamashita, N. Wachi, H. Omori, N. Fukui, T. Ikeue, H. Shinokubo, *Chem. – A Eur. J.* **2019**, *25*, 15580–15585.
[29] D. W. J. McCallien, J. K. M. Sanders, *J. Am. Chem. Soc.* **1995**, *117*, 6611–6612.
[30] A. L. Balch, M. M. Olmstead, S. L. Phillips, *Inorg. Chem.* **1993**, *32*, 3931–3936.
[31] A. L. Balch, B. C. Noll, S. L. Phillips, S. M. Reid, E. P. Zovinka, *Inorg. Chem.* **1993**, *32*, 4730–4736.
[32] K. Yamashita, D. Hirano, K. Sugiura, *Eur. J. Inorg. Chem.* **2020**, *2020*, 3507–3516.
[33] S. Richert, J. Cremers, I. Kuprov, M. D. Peeks, H. L. Anderson, C. R. Timmel, *Nat. Commun.* **2017**, *8*, 14842.
[34] K. Yamashita, N. Kuramochi, H. Pham Qui Van, K. Furutani, T. Ogawa, K. Sugiura, *Chempluschem* **2020**, *85*, 217–226.
[35] K. Yamashita, K. Kataoka, M. S. Asano, K. Sugiura, *Org. Lett.* **2012**, *14*, 190–193.
[36] K. Yamashita, S. Sakamoto, A. Suzuki, K. Sugiura, *Chem. - Asian J.* **2016**, *11*, 1004–1007.
[37] K. Yamashita, K. Kataoka, S. Takeuchi, K. Sugiura, *J. Org. Chem.* **2016**, *81*, 11176–11184.
[38] K. Yamashita, K. Kataoka, H. Pham Qui Van, T. Ogawa, K. Sugiura, *Asian J. Org. Chem.* **2018**, *7*, 2468–2478.
[39] L. C. Gong, D. Dolphin, *Can. J. Chem.* **1985**, *63*, 406–411.
[40] M. J. Crossley, L. G. King, S. M. Pyke, *Tetrahedron* **1987**, *43*, 4569–4577.
[41] M. J. Crossley, L. G. King, S. M. Pyke, C. W. Tansey, *J. Porphyrins Phthalocyanines* **2002**, *6*, 685–694.
[42] M. C. Balaban, C. Chappaz-Gillot, G. Canard, O. Fuhr, C. Roussel, T. S. Balaban, *Tetrahedron* **2009**, *65*, 3733–3739.
[43] A. A. Ryan, S. Plunkett, A. Casey, T. McCabe, M. O. Senge, *Chem. Commun.* **2014**, *50*, 353–355.
[44] C. H. Devillers, S. Hebié, D. Lucas, H. Cattey, S. Clément, S. Richeter, *J. Org. Chem.* **2014**, *79*, 6424–6434.
[45] Q. Chen, Y.-Z. Zhu, Q.-J. Fan, S.-C. Zhang, J.-Y. Zheng, *Org. Lett.* **2014**, *16*, 1590–1593.
[46] K. P. Birin, Y. G. Gorbunova, A. Y. Tsivadze, A. G. Bessmertnykh-Lemeune, R. Guilard, *Eur. J. Org. Chem.* **2015**, *2015*, 5610–5619.
[47] M. Kielmann, K. J. Flanagan, K. Norvaiša, D. Intrieri, M. O. Senge, *J. Org. Chem.* **2017**, *82*, 5122–5134.
[48] L. Schoepff, L. Kocher, S. Durot, V. Heitz, *J. Org. Chem.* **2017**, *82*, 5845–5851.
[49] A. L. Kieran, A. D. Bond, A. M. Belenguer, J. K. M. Sanders, *Chem. Commun.* **2003**, 2674–2675.
[50] H. Ding, X. Meng, X. Cui, Y. Yang, T. Zhou, C. Wang, M. Zeller, C. Wang, *Chem. Commun.* **2014**, *50*, 11162–11164.
[51] S. Nasri, I. Zahou, I. Turowska-Tyrk, T. Roisnel, F. Loiseau, E. Saint-Amant, H. Nasri, *Eur. J. Inorg. Chem.* **2016**, *2016*, 5004–5019.
[52] S. K. Samanta, D. Samanta, J. W. Bats, M. Schmittel, *J. Org. Chem.* **2011**, *76*, 7466–7473.
[53] C. Cao, Z. Zhou, Z. Yin, Q. Liu, *Org. Lett.* **2009**, *11*, 1781–1784.
[54] J. Taesch, V. Heitz, F. Topić, K. Rissanen, *Chem. Commun.* **2012**, *48*, 5118–5120.
[55] K. Hirose, *J. Inclusion Phenom. Macrocyclic Chem.* **2001**, *39*, 193–209.
[56] Y. Ide, T. Kuwahara, S. Takeshita, R. Fujishiro, M. Suzuki, S. Mori, H. Shinokubo, M. Nakamura, K. Yoshino, T. Ikeue, *J. Inorg. Biochem.* **2018**, *178*, 115–124.
[57] F. A. Walker, in *Handbook of Porphyrin Science, Vol. 6* (Eds.: K.M. Kadish, K.M. Smith, R. Guilard), World Scientific Publishing, Singapore, **2010**, pp. 1–337.
[58] S. Thies, H. Sell, C. Bornholdt, C. Schütt, F. Köhler, F. Tuczek, R. Herges, *Chem. - Eur. J.* **2012**, *18*, 16358–16368.
[59] M. Dommaschk, C. Schütt, S. Venkataramani, U. Jana, C. Näther, F. D. Sönnichsen, R. Herges, *Dalton Trans.* **2014**, *43*, 17395–17405.
[60] M. Kawao, H. Ozawa, H. Tanaka, T. Ogawa, *Thin Solid Films* **2006**, *499*, 23–28.
[61] G. M. Sheldrick, *Acta Crystallogr. Sect. A Found. Adv.* **2015**, *71*, 3–8.
[62] G. M. Sheldrick, *Acta Crystallogr. Sect. C Struct. Chem.* **2015**, *71*, 3–8.

Entry for the Table of Contents

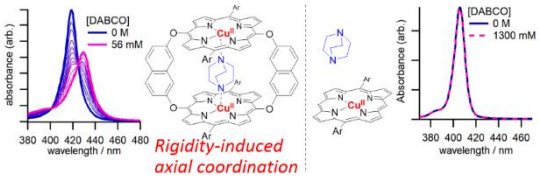

The unusual axial coordination on Cu^{II} and Ni^{II} ions in the cofacial cyclic porphyrin dimer was induced by its remarkably high structural rigidity without the assistance of electron-withdrawing substituents or strongly coordinating metal ions such as Zn^{II} porphyrins.